

# $\gamma$ -Aminobutyric A Receptor (GABA<sub>A</sub>R) Regulates Aquaporin 4 Expression in the Subependymal Zone

## RELEVANCE TO NEURAL PRECURSORS AND WATER EXCHANGE\*

Received for publication, October 15, 2014, and in revised form, December 21, 2014. Published, JBC Papers in Press, December 24, 2014, DOI 10.1074/jbc.M114.618686

Yuting Li<sup>†1</sup>, Udo Schmidt-Edelkraut<sup>‡</sup>, Fabian Poetz<sup>†2</sup>, Ilaria Oliva<sup>‡</sup>, Claudia Mandl<sup>‡</sup>, Gabriele Hölzl-Wenig<sup>‡</sup>, Kai Schönig<sup>§</sup>, Dusan Bartsch<sup>§</sup>, and Francesca Ciccolini<sup>†3</sup>

From the <sup>†</sup>Department of Neurobiology, Interdisciplinary Center for Neurosciences, University of Heidelberg, Im Neuenheimer Feld 364, 69120 Heidelberg and the <sup>§</sup>Department of Molecular Biology, Central Institute of Mental Health, Medical Faculty Mannheim/Heidelberg University, J5 Mannheim, Germany

**Background:** GABA<sub>A</sub>Rs regulate osmotic tension in prominin<sup>+</sup> neural stem cells and ependymal cells.

**Results:** GABA<sub>A</sub>R activation increases surface expression of AQP4, thereby affecting water exchange between the subependyma and the lateral ventricle.

**Conclusion:** Modulation of AQP4 expression by GABA underlies the osmotic function of the neurotransmitter.

**Significance:** GABA<sub>A</sub>Rs contribute to the regulation of water exchange between lateral ventricle and subependyma.

Activation of  $\gamma$ -aminobutyric A receptors (GABA<sub>A</sub>Rs) in the subependymal zone (SEZ) induces hyperpolarization and osmotic swelling in precursors, thereby promoting surface expression of the epidermal growth factor receptor (EGFR) and cell cycle entry. However, the mechanisms underlying the GABAergic modulation of cell swelling are unclear. Here, we show that GABA<sub>A</sub>Rs colocalize with the water channel aquaporin (AQP) 4 in prominin-1 immunopositive (P<sup>+</sup>) precursors in the postnatal SEZ, which include neural stem cells. GABA<sub>A</sub>R signaling promotes AQP4 expression by decreasing serine phosphorylation associated with the water channel. The modulation of AQP4 expression by GABA<sub>A</sub>R signaling is key to its effect on cell swelling and EGFR expression. In addition, GABA<sub>A</sub>R function also affects the ability of neural precursors to swell in response to an osmotic challenge *in vitro* and *in vivo*. Thus, the regulation of AQP4 by GABA<sub>A</sub>Rs is involved in controlling activation of neural stem cells and water exchange dynamics in the SEZ.

In the subependymal zone (SEZ),<sup>4</sup> the largest neurogenic region in the adult murine brain, neural stem cells (NSCs) give rise to neuroblasts throughout adulthood (1). Adult NSCs contact the blood vessels at the basal cell side and extend a primary cilium into the lateral ventricle at the apical side (2). The polar-

ized structure of NSCs is reflected by the expression of prominin-1 at the tip of the primary cilium (3). Although they are largely quiescent, prominin-1 immunopositive (P<sup>+</sup>) NSCs can undergo activation and enter the cell cycle in normal conditions and upon injury (4). Activated NSCs and transit-amplifying precursors (TAPs) express high levels of the epidermal growth factor receptor (EGFR) at the cell surface (E<sup>high</sup>), and they proliferate *in vivo* and *in vitro* in response to EGF (5). Because EGFR is progressively down-regulated during the differentiation of intermediate progenitors into neuroblasts (6), prominin-1 and EGFR represent useful markers for the efficient identification and isolation of activated NSCs and TAPs (7–9).

In the pre- and postnatal SEZ, the inhibitory neurotransmitter  $\gamma$ -aminobutyric acid (GABA) through the activation of its type A receptors (GABA<sub>A</sub>Rs) affects multiple aspects of neurogenesis, including proliferation of the various precursor types, cell migration, and differentiation (10–12). In neuroblasts, GABA<sub>A</sub>R-induced cell depolarization was consistently found to decrease proliferation and migration (13, 14). In contrast, the effect of GABA<sub>A</sub>R activation on the proliferation of NSCs and TAPs is still debated (15). The multiple effects elicited by GABA<sub>A</sub>R activation are likely a consequence of the differences in magnitude and direction of the anionic GABAergic currents. In primary precursors, they are small and hyperpolarizing leading to osmotic swelling, whereas the GABAergic currents increase in magnitude and turn depolarizing in differentiating neuroblasts (16–18).

Aquaporins (AQPs), provide a major pathway for osmotically driven water transport through cell membranes. AQP4, the predominant isoform in the central nervous system, is extensively expressed in adult neurogenic regions such as the SEZ, especially in ependymal cells and subependymal astrocytes (19). Adult NSCs express AQP4 (20), and genetic ablation of AQP4 affected multiple aspects of NSC function, including proliferation (21). However, the molecular mechanisms underlying the effects of AQP4 on NSCs are still unclear.

Genetic ablation of AQP4 expression leads to a marked reduction of water uptake through the blood-brain barrier (22)

\* This work was supported by a grant from the Deutsche Forschungsgemeinschaft.

<sup>1</sup> Present address: Helmholtz Young Investigator Group, Normal and Neuroplastic CNS Stem Cells, German Cancer Research Center (DKFZ), DKFZ-ZMBH Alliance, Im Neuenheimer Feld 581, 69120 Heidelberg, Germany.

<sup>2</sup> Present address: Helmholtz Young Investigator Group, Posttranscriptional Control of Gene Expression, German Cancer Research Center (DKFZ), Heidelberg, Germany, and Zentrum für Molekulare Biologie der Universität Heidelberg (ZMBH), Germany.

<sup>3</sup> To whom correspondence should be addressed. Tel.: 49-6221-548696; Fax: 49-6221-546700; E-mail: Ciccolini@nbio.uni-heidelberg.de.

<sup>4</sup> The abbreviations used are: SEZ, subependymal zone; NSC, neural stem cell; AQP, aquaporin; EGFR, EGF receptor; ANOVA, analysis of variance; Cal-C, calphostin C; TAP, transit amplifying precursor; PLA, proximity ligation assay; NBA, neurobasal; FSC, forward scattering; BFA, brefeldin-A; qRT, quantitative reverse transcription.

## GABA Regulates AQP4 in the SEZ

and of brain swelling following cytotoxic brain edema (23, 24). The expression of AQP4 is not constant but is functionally regulated at the levels of both transcription and channel assembly (25–27). Phosphorylation of AQP4 has been consistently reported as a mechanism underlying the regulation of channel assembly as well as water permeability (28, 29). Nevertheless, little is known concerning the regulation of AQP4 expression in the SEZ lineage and the relationship between osmolarity and neurogenesis.

In this study, we provide evidence that within the SEZ GABA<sub>A</sub>R signaling modulates the expression of AQP4 at the cell surface. We show that the GABAergic-dependent osmotic regulation in this region affects EGFR expression in neural precursors and water uptake upon osmotic challenge.

### MATERIALS AND METHODS

**Cell Sorting and Culture**—Neonatal (P7) and adult (P56) C57B6 mice were killed by decapitation and cervical dislocation after CO<sub>2</sub> inhalation, respectively, in accordance with the local ethical guidelines for the care and use of laboratory animals (Karlsruhe, Germany). The AQP4 knock-out (KO) mice were generated as described previously (24). The whole SEZ of the lateral ventricle was dissected and dissociated in sucrose solution (150 mM sucrose, 125 mM NaCl, 3.5 mM KCl, 1.2 mM NaH<sub>2</sub>PO<sub>4</sub>, 2.4 mM CaCl<sub>2</sub>, 1.3 mM MgCl<sub>2</sub>, 6.65 mM glucose, and 2 mM HEPES, pH 6.9, osmolarity 326 mM, all from Sigma), and cells were processed for sorting as already described (17). Briefly, after enzymatic tissue dissociation, cells were incubated with prominin-1-APC antibodies (Miltenyi Biotec) and then stained with Alexa488-tagged EGF (EGF-A; 20 ng/ml) (Molecular Probes) and 1 μg/ml propidium iodide, 0.001% DNase (all from Sigma). Before sorting, bicuculline methobromide (50 μM) (Biotrend) was added to dissection and sort solution for 30 min.

After sorting, cells were plated on Matrigel-coated 12-well chamber slides (Ibidi) in neurobasal (NBA) (Invitrogen) media, 2% B27, 2 mM L-glutamine, penicillin 100 units/ml, 100 μg/ml streptomycin (all from Sigma), 10 ng/ml FGF-2 (PeproTech) and analyzed by live imaging or were fixed and processed for immunocytochemistry after 6 or 24 h, as described in the text. Neurosphere cultures were established from the dissociated SEZ of WT and AQP4 KO neonatal mice in NBA medium supplemented with 2% B27, 10 ng/ml FGF-2, and 20 ng/ml EGF-2 (PeproTech), as described previously (17).

**Immunocytofluorescence**—Cells were fixed and immunostained with or without previous permeabilization as described previously (30). Before fixation, and 6 h after plating, cells were incubated with bicuculline (50 μM, up to 30 min) or muscimol (25 μM, up to 15 min), with or without 30 min of pretreatment with brefeldin-A (BFA 3 μg/ml) as described in the text.

Primary antibodies were detected using Alexa 488- or Cy3-conjugated secondary antibodies (Molecular Probes). Rabbit polyclonal to AQP4 (Abcam, 1:500), mouse monoclonal to GABA<sub>A</sub>R β-chain antibody (Chemicon 1:200), and EGFR (Sigma, 1:200) primary antibodies were used on permeabilized or nonpermeabilized cell and tissue sections, as indicated. Nuclei were counterstained with 4,6-diamidino-2-phenylindol dihydrochloride (DAPI) 1:1000 (Roche Diagnostics).

Immunopositive cells were quantified from at least three independent experiments by analyzing an average of 300 cells across multiple fields with a conventional fluorescence microscope (DMIRBE Microscope; Leica, Germany). Changes in expression were evaluated by calculating the number of immunopositive cells as percentage of DAPI.

**Immunohistochemistry**—Adult mice were deeply anesthetized by intraperitoneal injection of sodium pentobarbital (2 ml/kg body weight; Narcoren®, Merck, Germany) and perfused transcardially with 4% paraformaldehyde in 0.1 M phosphate buffer. Brains were post-fixed overnight in 4% paraformaldehyde at 4 °C and transferred into a 20% sucrose solution. After embedding in 4% low melting agarose, 30-μm thick coronal vibratome sections were cut and processed for immunohistochemistry. Image acquisition and analysis were done as described previously (17).

**Immunoprecipitation and Western Blot**—Lysates of homogenized tissue were obtained in Membrane extraction buffer (5 mM HEPES, 0.32 M sucrose, 0.1 mM EDTA) and/or whole cell lysis buffer (50 mM HEPES, 150 mM NaCl, 1% Triton X-100, 2 mM EDTA, 0.5 mM DTT, pH 7.4) supplemented with Phospho-Stop (Sigma) and protease inhibitor mixture complete (Roche Diagnostics). Cell extracts (300 μg) were immunoprecipitated with AQP4 antibody (2 μg) using Dynabeads Protein G (Novex). Finally, proteins were fractionated by SDS-PAGE and incubated with antibodies to AQP4 (Abcam 1:1000) or to phosphoserine (Millipore, 1:500).

**Proximity Ligation Assay**—Proximity ligation assay (PLA) was used to visualize *in situ* protein interaction (31) and protein phosphorylation (32) because it is based on dual recognition of epitopes, which can be detected only if they are localized less than 40 nm apart. Here, we used PLAs to investigate the proximity of AQP4 and GABA<sub>A</sub>R and changes in serine phosphorylation associated with AQP4. PLAs were performed using the Duolink kit (Olink Bioscience, Uppsala, Sweden). Briefly, isolated precursor cells or brain slices were blocked with 5% diluted FCS for 30 min at room temperature. Antibodies against AQP4, in combination with either GABA<sub>A</sub>R or phosphoserine antibodies, were diluted in PBS containing 1% FCS at suitable concentrations and were incubated overnight at 4 °C. Oligonucleotide-bound secondary antibodies and additional oligonucleotides were ligated for the generation of a circular DNA substrate that was amplified and detected by means of fluorescent complementary oligonucleotides according to the manufacturer's instructions. Quantitative analysis was done by calculating the percentage of cells displaying fluorescent dots, revealing colocalization of the primary antibodies. Alternatively, when indicated in the text, cells were subdivided into groups based on the number of the displayed fluorescent signals, and the effect of the treatment was quantified by calculating the percentage of the total cells in each group.

**Brain Surgery**—Mice were fully anesthetized and set into a stereotaxic frame. Vaseline was placed over the eyes of the animals to prevent them from drying. Mice were given bilateral intraventricular injection with 1.2 μl of vehicle, bicuculline (30 pmol), muscimol (3 nmol), or hypo-osmotic solution at a rate of 0.4 μl/min with a 33-gauge stainless steel guided cannula. The following stereotaxic coordinates were used to target the lat-

eral ventricle on both sides of the brain: AP = 0 mm, ML =  $\pm$ 1.2 mm, V = -2.0 mm from the bregma. The cannula was left in place for 5 min following the injection. Mice were sacrificed 30–60 min after the injection and were processed for immunohistochemistry or water retention experiments.

**Measurement of Tissue Water Content**—After dissection, the tissue was supersonicated in tubes. The tubes containing the different tissue samples were weighted before and after drying in a Fiestream vacuum oven for 24 h at 80 °C and -1.000 mbar. Brain water accumulation was calculated by comparing values for baseline brain water content with the tissue water content after treatment. The percentage of water content per tissue sample was calculated as (wet mass - dry mass)  $\times$  100/(wet mass) (22).

**Osmotic Swelling and Cell Size Measurements**—For osmotic swelling measured by live imaging, the sorted cells were loaded with calcein-AM (1  $\mu$ M) (Invitrogen) diluted in Hanks' buffered salt solution (HBSS, 1.3 mM CaCl<sub>2</sub>, 0.5 mM MgCl<sub>2</sub>, 0.4 mM MgSO<sub>4</sub>, 5.4 mM KCl, 0.44 mM KH<sub>2</sub>PO<sub>4</sub>, 4.2 mM NaHCO<sub>3</sub>, 137 mM NaCl, 0.25 mM Na<sub>2</sub>HPO<sub>4</sub>, and 5.6 mM glucose) for 30 min at 37 °C. Recordings were performed at 37 °C in an open-topped perfusion chamber (Life Imaging Service, Switzerland) mounted in an inverted fluorescent microscope (IX70 Olympus, Germany) equipped with a CCD camera (ImagoQE, TILL Photonics GmbH, Germany) and a software interface (TILLvisION 4.0, TILL Photonics GmbH, Germany). Excitation light of 390 nm was generated by a monochromator (Polychrom IV, TILL Photonics GmbH, Germany) coupled to a xenon short arc light source (USHIO, Japan). After incubation with bicuculline (50  $\mu$ M, up to 30 min) or muscimol (25  $\mu$ M, up to 15 min), as indicated in the text, cultures were treated with hypo-osmotic (200 mosM/kg), hyper-osmotic (400 mosM/kg), or iso-osmotic solution (300 mosM/kg) as control for an additional 30 min. Different osmolarity reflected variations in NaCl or D-gluconic acid sodium salt used to obtain hyper-osmotic Cl<sup>-</sup> free solution. Recordings were performed after the cells had adapted to the environment for 15–20 min. Images were taken every 10 s. Changes in cell size were calculated using ImageJ software. All data came from at least three independent experiments from different cell preparations.

For volume analysis by spinning disk confocal microscopy, sorted P<sup>+</sup> cells were treated with bicuculline (50  $\mu$ M) or left untreated as control for 30 min at 37 °C before loading with wheat germ agglutinin-Alexa 488 (5  $\mu$ g/ml) (Invitrogen) for 10 min. After rinsing with pre-warmed HBSS, the cells were incubated at 37 °C for a further 15 min before fixation. Images of confocal sections were taken every 0.15  $\mu$ m using a spinning-disk confocal system, merged together and converted by deconvolution methods. Changes in cell size were calculated using ImageJ software. All data were collected from 20 to 30 cells from three independent experiments from different cell preparations. Osmotic swelling was also measured by flow cytometry in cell suspensions. Changes in forward scattering (FSC) reflected variations in the osmolarity of the medium and were analyzed using FACSDiva 6.1.3. FACS histograms illustrating the frequency distribution of FSC were fitted with SigmaPlot by single Gaussian functions whose mean, S.D., and adjusted R-squared values were calculated. The statistical significance of

the variations between control and treated groups was calculated using Student's *t* test.

**Quantitative Reverse Transcription-PCR**—Cells were sorted into lysis buffer, and the total RNA was extracted with RNeasy micro kit (Qiagen). Total RNA was reversely transcribed using oligo(dT) primers and Moloney murine leukemia virus reverse transcriptase, RNase H Minus (all from Promega). TaqMan probes for genes of interest were purchased from Applied Biosystems. The quantitative reverse transcription (qRT)-PCR was performed in 7300 Real Time PCR system from Applied Biosystems. Cycle threshold (*Ct*) values were obtained from the logarithmic phase of the amplification plot between normalized fluorescence of a Fam reporter dye for the TaqMan MGB probe and cycle numbers for the PCR. *Ct* values for the genes of interest were normalized against  $\beta$ -actin. Expression levels of the genes of interest in different cell types were normalized to P<sup>-</sup>/E<sup>low</sup> cells.

**Statistical Analysis**—The data are represented as means  $\pm$  S.E. and analyzed using SigmaStat 3.5 or analysis of live imaging experiments means of averaged values for each time point were compared between control and treatment. In the figure are given the highest *p* values obtained. Statistical significance was determined by one-way analysis of variance (ANOVA) for multiple comparisons followed by Bonferroni post hoc test or the two-tailed Student's *t* test using a statistical package (GraphPad Prism). Calculated *p* values are indicated in the figure as follows: \* and #, *p*  $\leq$  0.05; \*\* and ##, *p*  $\leq$  0.01; \*\*\* and ###, *p*  $\leq$  0.001.

## RESULTS

**Colocalization of GABA<sub>A</sub>Rs and AQP4 in SEZ Precursors**—Previous studies have shown that AQP4 is expressed in neurosphere cultures derived from adult murine and human neural precursors (20). However, the distribution of AQP4 in the different precursor types of the SEZ is still unknown. To investigate this issue, we used flow cytometry to measure expression levels of EGFR and prominin-1 and purify the following cell populations from the SEZ of neonatal mice: P<sup>+</sup>/E<sup>low</sup> cells consisting of ependymal cells and quiescent NSCs; P<sup>+</sup>/E<sup>high</sup> cells being highly enriched in activated NSCs; P<sup>-</sup>/E<sup>high</sup> cells enriched in TAPs and pre-neuroblasts; and P<sup>-</sup>/E<sup>low</sup> cells representing mostly neuroblasts (7, 9, 17).

To investigate the relationship between GABA<sub>A</sub>Rs and water channels, we first analyzed the expression of AQP4 in these four populations. Analysis by qRT-PCR revealed increased mRNA levels in P<sup>+</sup> cells. In particular, P<sup>+</sup>/E<sup>high</sup>-activated NSCs contained approximately six times more *Aqp4* transcripts than isolated neuroblasts and P<sup>-</sup>/E<sup>high</sup> cells (Fig. 1A). A similar expression pattern was also observed upon analysis of AQP4 protein by immunofluorescence, showing an increased number of immunopositive cells and higher levels of fluorescence in the sorted P<sup>+</sup> cells than in the remaining P<sup>-</sup> populations (Fig. 1B). As we had previously found that neural precursors display benzodiazepine-sensitive GABA<sub>A</sub>Rs, we next investigated by qRT-PCR the expression of GABA<sub>A</sub>R  $\alpha$  subunits (*gabra*) 1, 2, 3, and 5, which confer high affinity binding of benzodiazepines, and of *gabra* 4 and GABA<sub>A</sub>R  $\delta$  subunits (*gabrd*), which are not associated with benzodiazepine sensitivity. We selected these sub-

## GABA Regulates AQP4 in the SEZ

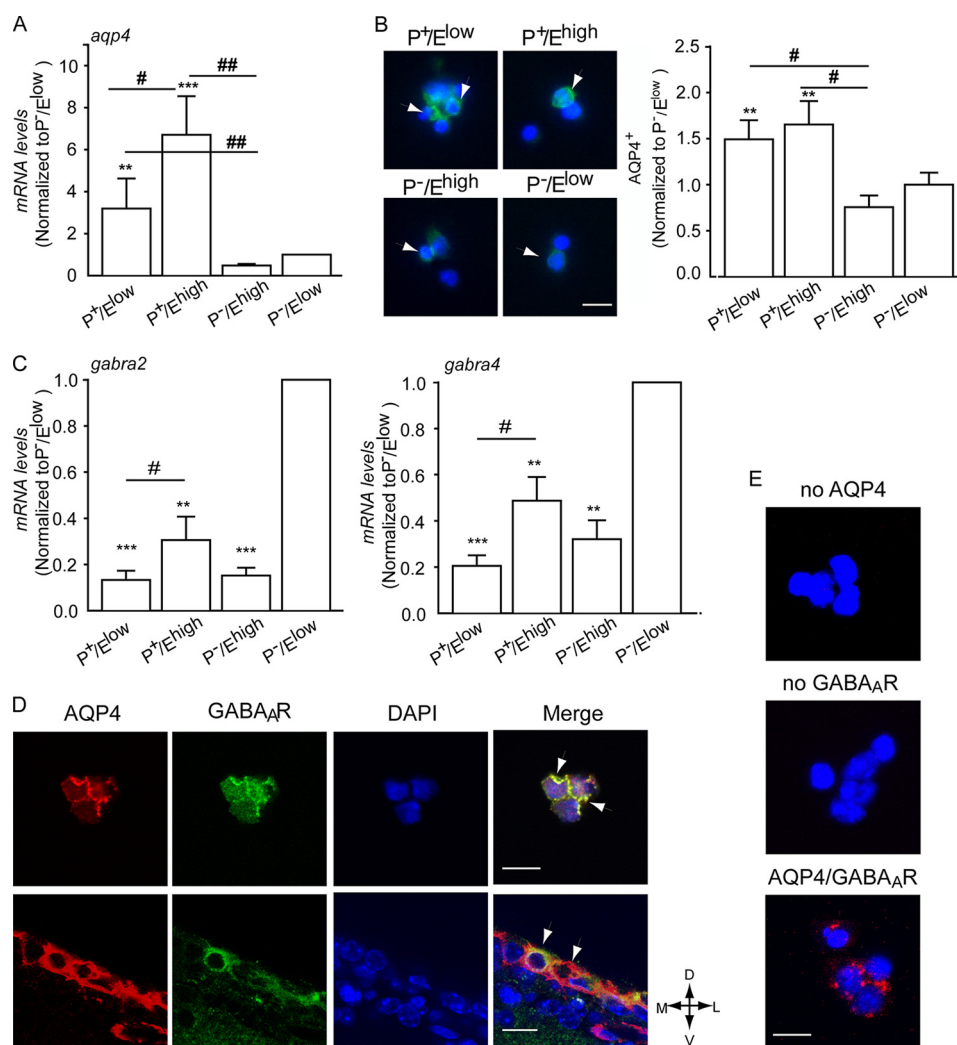


**FIGURE 1. GABA<sub>A</sub>Rs and AQP4 are coexpressed in close proximity to SEZ precursors.** A–C, analysis of levels of *Aqp4* transcripts (A), AQP4 immunoreactivity (B), and transcripts for the indicated GABA<sub>A</sub>R subunits (C) in the given sorted populations. For transcript quantification, values are the means of relative expression levels from *ddCT* ± S.E. normalized to P<sup>-</sup>/E<sup>low</sup> cells. \* indicates significantly different from P<sup>-</sup>/E<sup>low</sup> cells (ANOVA), *n* = 4. B, left panels show representative photomicrographs of sorted nonpermeabilized cells illustrating AQP4 immunoreactivity (green) and DAPI counterstaining of the nuclei (blue). Scale bar, 10 μm. D, representative confocal photomicrographs of postnatal SEZ-dissociated cells (upper panel) and adult coronal slices (lower panel) upon double immunostaining without previous permeabilization. Scale bar, 15 μm. Arrowheads point to double immunopositive cells. D, dorsal; M, medial; L, lateral; V, ventral. E, representative photomicrographs of sorted P<sup>+</sup> cells illustrating AQP4 and GABA<sub>A</sub>R colocalization (red) detected by PLAs upon incubation with the indicated primary antibodies and DAPI (blue) counterstaining of the nuclei. Scale bar, 15 μm.

units because our previous analyses (17) had revealed that they were all expressed at very low levels in neural precursors. Indeed, transcript levels for all genes analyzed were significantly lower within the remaining populations than in purified P<sup>-</sup>/E<sup>low</sup> neuroblasts. Although *gabra2* and *gabra4* were detected in all isolated populations (Fig. 1C), transcripts for the subunits *gabrd* and the remaining *gabra* subunits were not detected in P<sup>+</sup>/E<sup>high</sup>-activated NSCs (data not shown). This suggests that *gabra2* subunits are responsible for the sensitivity to benzodiazepines in the NSC compartment (17).

We next examined the localization of GABA<sub>A</sub>Rs and AQP4 by immunostaining. Immunoreactivities to AQP4 and GABA<sub>A</sub>Rs colocalized in dissociated neonatal SEZ cells (Fig. 1D, upper panel) and in coronal adult brain sections (Fig. 1D, lower panel). The detection of GABA<sub>A</sub>R and AQP4 antibodies by PLAs (Fig. 1E) generated a strong fluorescent signal confirming that GABA<sub>A</sub>Rs and AQP4 are localized in close proximity in P<sup>+</sup> precursors.

**GABA<sub>A</sub>R Regulates AQP4 Phosphorylation and Its Expression at the Cell Surface**—We next investigated the possibility that GABA<sub>A</sub>R signaling may affect AQP4 expression. As reported previously (17), 6 h after sorting and plating treatment with the GABA<sub>A</sub>R-specific antagonist bicuculline (50 μM) caused a reduction in the expression of both AQP4 (Fig. 2A) and EGFR (Fig. 2B) at the surface of sorted P<sup>+</sup> but not P<sup>-</sup> cells (data not shown). In addition, GABA<sub>A</sub>R blockade led to a 50% reduction in the colocalization of GABA<sub>A</sub>Rs and AQP4 (Fig. 2C) at the cell surface of P<sup>+</sup> cells as shown by PLAs. This decrease was not due to an effect of bicuculline on total cellular AQP4, as determined by permeabilization and immunostaining of either P<sup>+</sup> or P<sup>-</sup> cells (data not shown). Because in this system bicuculline also does not affect GABA<sub>A</sub>R expression (17), our data indicate that endogenous GABA<sub>A</sub>R signaling promotes the expression of AQP4 at the cell surface.

It has been reported that reversible phosphorylation of AQP4 results in allosteric changes, which in turn affect the expression

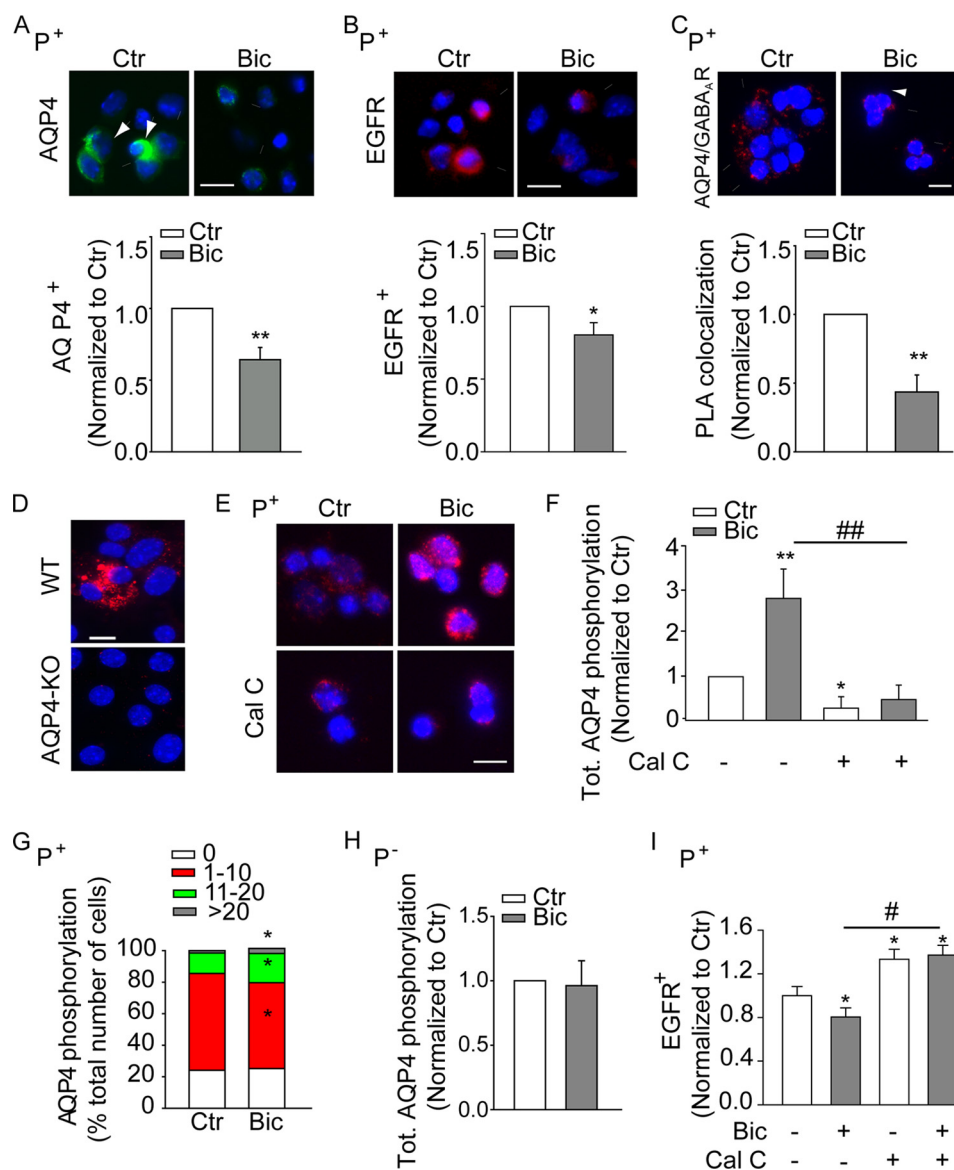


**FIGURE 2. Effect of GABA<sub>A</sub>R signaling on phospho-AQP4 and the expression of the water channel at the surface of precursors sorted from the neonatal (P7) SEZ.** *A* and *B*, upper panels show representative photomicrographs illustrating AQP4 (*A*) and EGFR (*B*) immunoreactivity and colocalization of AQP4 and GABA<sub>A</sub>R detected by PLAs (*C*) at the surface of sorted  $P^+$  precursors. Relative quantification is shown in the lower panels. *D* and *E*, representative microphotograph illustrating AQP4 serine phosphorylation by PLAs in permeabilized neurosphere cultures derived from WT and AQP4 knock out (KO) mice (*D*) and sorted  $P^+$  cells (*E*). Immunoreactivity and colocalization are visualized in red and DAPI counterstain of the nuclei in blue. Scale bars, 15  $\mu$ m (*A–C*) and 10  $\mu$ m (*D*). *F–H*, quantitative analysis of phospho-AQP4 by PLAs in sorted  $P^+$  and  $P^-$  cells as indicated. AQP4 primary antibodies were added with (*F–H*) and without (*G*) previous permeabilization to visualize total and surface phospho-AQP4, respectively. *G*, cells were categorized based on the number of the displayed fluorescent signals, and the effect of the treatment was quantified by calculating the number of cells in each group as percentage of the total. *I*, quantitative analysis of EGFR expression at the cell surface of sorted  $P^+$  cells by immunostaining. Sorted cells were exposed to bicuculline (Bic, 50  $\mu$ M for 30 min) and calphostin C (Cal-C, 1  $\mu$ M for 45 min) 6 h after culturing or left untreated (Ctr) as indicated. \* indicates significantly different from untreated cells (ANOVA)  $n \geq 3$ .

of the water channel at the cell surface (33, 34) and its water permeability (35). Therefore, we next investigated the effect of GABA<sub>A</sub>R function on serine phosphorylation of AQP4. Because of the unavailability of antibodies recognizing phosphorylated AQP4, for this analysis we took advantage of PLAs using antibodies to AQP4 and phosphoserine (32). Because this approach would detect phosphorylation on serine residues localized on AQP4 as well as on a closely (less than 40 nm) associated protein, hereafter we will use phospho-AQP4 to refer to either possibility. We first verified the specificity of this approach on neurosphere cultures established from WT and AQP4 KO mice. Fluorescent signals, showing colocalization of

the two antibodies, were only detected in neurosphere cultures obtained from WT mice (Fig. 2*D*) suggesting that our approach detects specifically changes in phospho-AQP4.

We therefore next took advantage of this method to investigate the effect of bicuculline on phospho-AQP4 in sorted cells. Treatment of sorted  $P^+$  cells with bicuculline led approximately to a 3-fold increase in total phospho-AQP4 (Fig. 2, *E* and *F*). The treatment also increased phospho-AQP4 in the water channel pool expressed at the surface of  $P^+$  cells, albeit at a much lower extent than in the total protein (Fig. 2*G*). In contrast, GABA<sub>A</sub>R blockade did not affect levels of phospho-AQP4 in  $P^-$  cells (Fig. 2*H*). It has been previously shown that PKC mediates phosphorylation of ser-

## GABA Regulates AQP4 in the SEZ

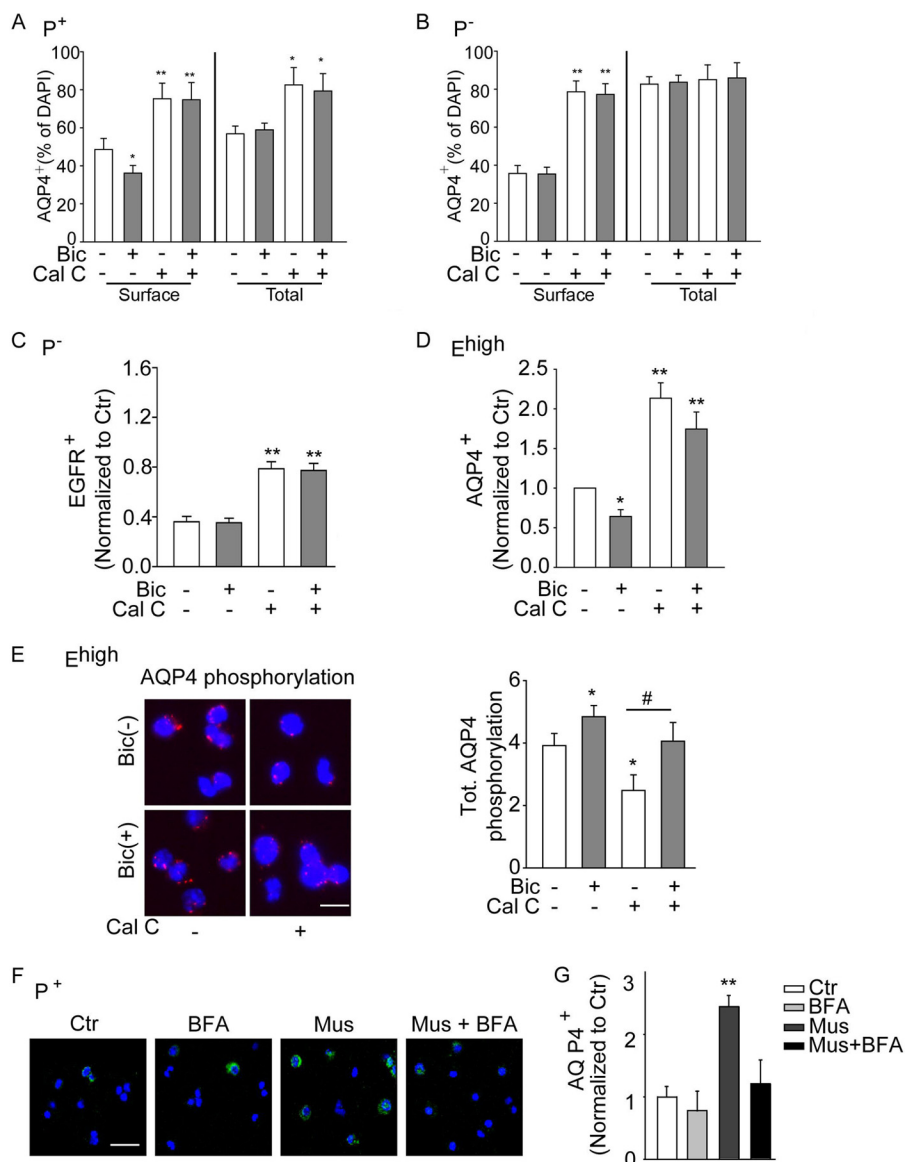


**FIGURE 3. PKC and GABA<sub>A</sub>R signaling affects AQP4 expression and its phosphorylation in precursors sorted from the neonatal (P7) SEZ based on prominin-1 or EGFR expression.** A–C, effect of bicuculline (Bic, 50 μM) and calphostin C (Cal-C, 1 μM) on the expression of AQP4 (A and B) and EGFR (C) in sorted P<sup>+</sup> and P<sup>-</sup> precursors as indicated. *n* ≥ 3. D, quantification of AQP4 expression at the cell surface of sorted EGFR<sup>high</sup> cells after treatment as indicated. *n* ≥ 3. E, analysis of phospho-AQP4 by PLAs in permeabilized sorted E<sup>high</sup> cells. Left column panels show representative photomicrographs of the cells and right column panels relative quantifications. Red fluorescent signals reveal phospho-AQP4. Scale bar, 10 μm. Six hours after sorting, cells were exposed to bicuculline (50 μM for 30 min) in the presence or absence of Cal-C (1 μM for 45 min) or left untreated (Ctr) as indicated. F, panels show representative photomicrographs illustrating AQP4 immunoreactivity at the surface of P<sup>+</sup> cells that after sorting had been plated for 6 h before treatment without (Ctr) or with muscimol (Mus) and/or brefeldin A (BFA) as indicated. Scale bar, 35 μm. G, quantification of the immunostaining in F. *n* ≥ 3. \* indicates significantly different from control untreated cells (ANOVA) \*, #, *p* < 0.05; \*\*, *p* < 0.01.

ine within the loop D region of AQP4 thereby affecting its function (28). Therefore, to further investigate the relationship between GABAergic regulation of AQP4 and EGFR expression, we next used calphostin C (Cal-C), a selective PKC inhibitor, to interfere with AQP4 phosphorylation and to modulate its expression at the cell surface. In sorted P<sup>+</sup> cells, exposure to Cal-C significantly reduced intracellular phospho-AQP4 (Fig. 2, E and F) and counteracted the effect of bicuculline on EGFR expression (Fig. 2J). Likewise, the Cal-C treatment also increased the expression of the water channel at the surface and, to a lesser extent, the total amount of intracellular AQP4 (Fig. 3A). In contrast to bicuculline, treatment with Cal-C had similar effects also on isolated P<sup>-</sup> cells, increasing the expression of AQP4 (Fig. 3B) and EGFR (Fig. 3C) at

the cell surface. Treatments with bicuculline and/or Cal-C also similarly affected AQP4 expression (Fig. 3D) and phosphorylation (Fig. 3E) in sorted E<sup>high</sup> cells, albeit to a lower degree. This is consistent with our previous observations concerning the effect of bicuculline on EGFR expression in this population (17).

Because GABA<sub>A</sub>R function mostly affected intracellular phospho-AQP4 (see for comparison Fig. 2, F and G), we postulated that it may modulate the recruitment of the water channel at the cell surface. Therefore, we next investigated the effect of the GABA<sub>A</sub>R agonist muscimol on the expression of AQP4 at the surface of sorted P<sup>+</sup> cells, which had been either exposed for 30 min to BFA (36), to prevent the anterograde movement of AQP4 from the cis-Golgi to the cell membrane, or left

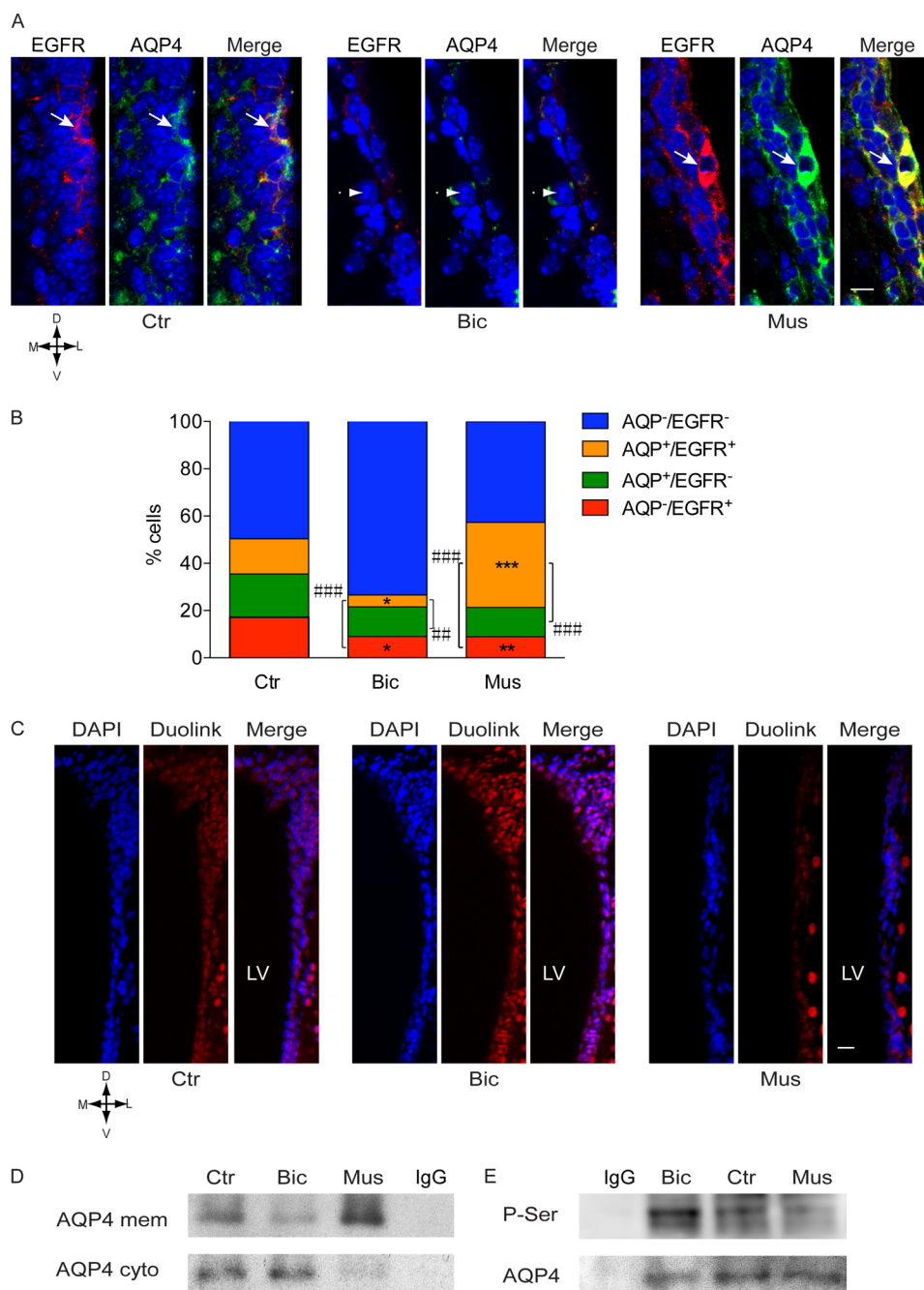


**FIGURE 4. GABA<sub>A</sub>Rs positively regulate AQP4 expression and its phosphorylation *in vivo*.** *A*, confocal photomicrographs of coronal sections of the adult SEZ illustrating representative examples of immunostaining as indicated and DAPI (blue) counterstaining of the nuclei. *A*, mice were microinjected (i.v.) with vehicle (*Ctrl*), bicuculline (*Bic*, 30 pmol) and muscimol (*Mus*, 3 nmol). Immunolabeling was performed without permeabilization. Scale bar, 15  $\mu$ m. *B*, quantitative analysis of the immunostaining in *A*. \* indicates significantly different from the control counterpart in each single and double immunopositive population. # indicates significantly different from the control counterpart in total cells immunopositive for EGFR and AQP4 as indicated (ANOVA);  $n \geq 6$  mice/group. *C*, confocal photomicrographs illustrating representative examples of total phospho-AQP4 (red) in the adult SEZ revealed by PLAs and DAPI counterstaining of the nuclei after exposure to vehicle, bicuculline, or muscimol as indicated. *D*, dorsal; *M*, medial; *L*, lateral; *V*, ventral. Scale bar, 25  $\mu$ m. *D*, plasma membrane (*mem*) and remaining (*cyto*) fraction of dissociated SEZ tissue stained for AQP4 after indicated treatments shown by immunoprecipitation and immunoblots. *E*, whole cell extracts of dissociated SEZ tissue upon the indicated treatments were immunoprecipitated with AQP4 antibody, and immunoblots were stained with antibodies to phosphoserine (*P-Ser*) and AQP4.

untreated as control. In line with our previous findings, forced activation of GABA<sub>A</sub>Rs greatly enhanced the expression of AQP4 at the cell surface (Fig. 3, *F* and *G*). Pretreatment with BFA did not affect surface expression of AQP4, although it completely abolished the effect of muscimol (Fig. 3, *F* and *G*).

Taken together, these data show that the modulation of surface AQP4 requires intact anterograde transport, indicating

that the change in phosphorylation may affect the anterograde transport of the protein. Our data also indicate that the GABAergic regulation of AQP4 expression contributes to the effect of GABA<sub>A</sub>Rs on osmotic tension and expression of EGFR at the surface of neural precursors.

*GABA<sub>A</sub>R Activation Regulates AQP4 and EGFR in Vivo*—We next investigated whether endogenous GABA<sub>A</sub>R signaling had

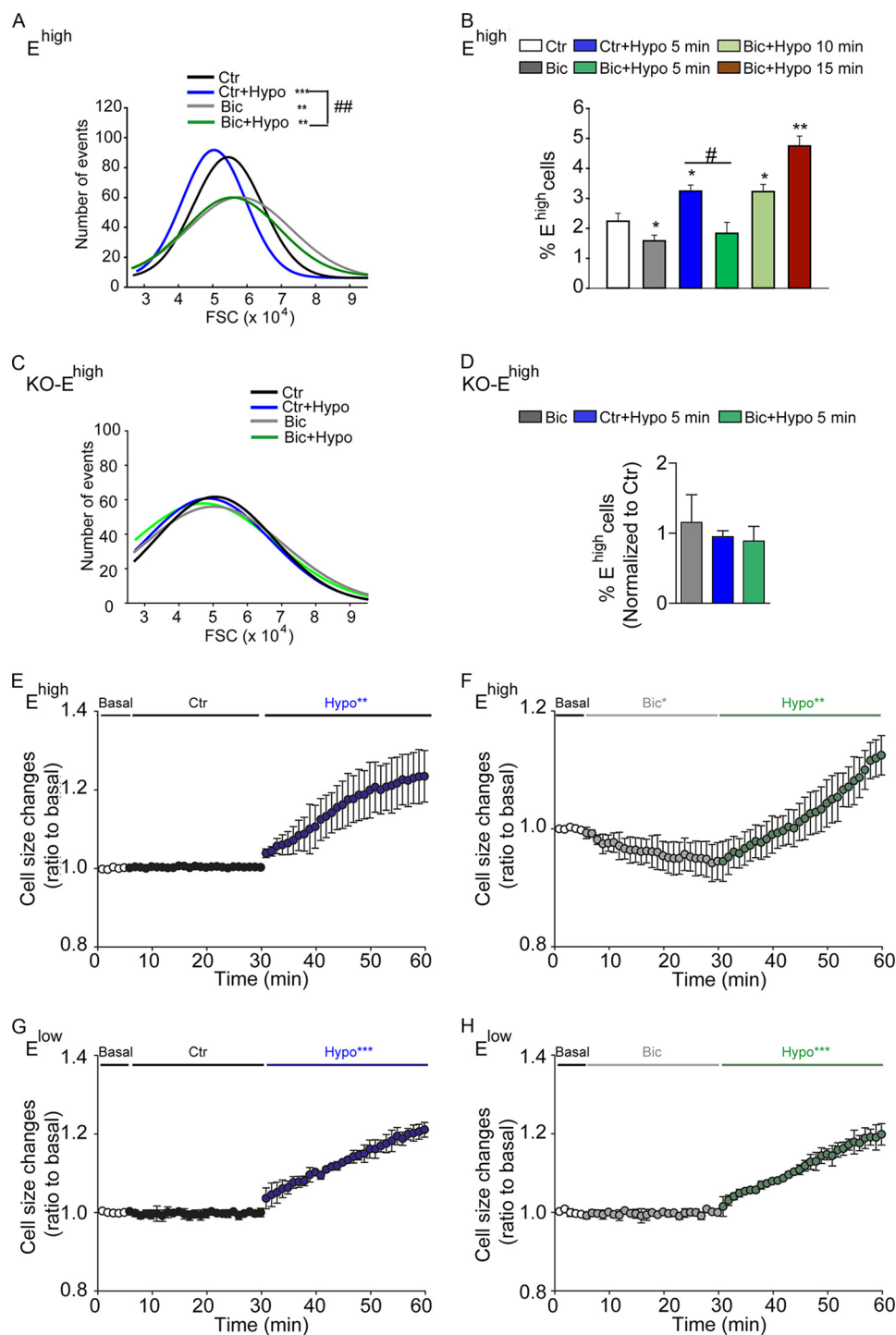


**FIGURE 5. Blockade of GABA<sub>A</sub>Rs delays swelling of  $E^{\text{high}}$  cells in response to osmotic challenge.** A and D, effect of GABA<sub>A</sub>Rs on the response to osmotic challenge of dissociated cells derived from the neonatal SEZ of neonatal WT (A and B) and AQP4 KO (C and D) mice. Representative FACS histograms illustrating the frequency distribution of forward side scattering (FSC) values of  $E^{\text{high}}$  cells are shown in B and C, quantification of the number of  $E^{\text{high}}$  cells upon the indicated treatments are given in B and D. Curves were fitted by single Gaussian functions whose mean, S.D., and adjusted *R*-squared values were calculated. FSC was analyzed on freshly dissociated cells that had been treated with (Bic) or without (Ctr) bicuculline during dissection and staining for 30 min. Five minutes before FACS analysis, hypo-osmotic solution (with the final osmolarity of 200 mosM/kg) was added to the control (Ctr+Hypo) and bicuculline (Bic+Hypo) group as indicated. \* indicates significantly different from control (ANOVA); \*\*, ##,  $p < 0.01$ ; \*\*\*,  $p < 0.001$ , ANOVA;  $n \geq 4-5$ . E-H, effect of GABA<sub>A</sub>Rs on the response to osmotic challenge of neonatal  $E^{\text{high}}$  (E and F) and  $E^{\text{low}}$  (G and H) cells that after sorting were cultured in NBA medium for 2 days before loading with calcein-AM (1  $\mu\text{M}$ ) and live imaging. Cells were exposed to bicuculline (50  $\mu\text{M}$ ) or left untreated as control (Ctr) and were recorded for 25 min as indicated. Thereafter, hypo-osmotic solution (Hypo, 200 mosM/kg) supplemented with or without bicuculline (50  $\mu\text{M}$ ) was added, and cells were recorded for an additional 30 min. Changes in cell size are represented as mean  $\pm$  S.D.  $n \geq 3$ . \*,  $p < 0.05$ ; \*\*,  $p < 0.01$ ; \*\*\*,  $p < 0.001$ . Values of the mean curve obtained in basal and treatment (Ctr-Hypo, Bic-Hypo) conditions were averaged every 60 s and analyzed by two-tailed Student's *t* test.

a similar effect on the regulation of AQP4 expression within the adult SEZ niche. Mice were microinjected intraventricularly (i.v.) with vehicle as control or either bicuculline or muscimol to inhibit or activate GABA<sub>A</sub>Rs, respectively. After 30 min, mice were sacrificed, and thereafter the brain slices were either immunostained to investigate expression of AQP4 and EGFR or processed for PLAs to determine phospho-AQP4. In vehicle-microinjected animals, a similar number of cells expressed either or both antigens at the cell surface, and they were mainly localized at the apical side of the border (Fig. 4, A and B). Consistent with our analysis *in vitro*, injection of bicuculline led to a decrease in the number of all immunopositive populations, which was significant for cells expressing EGFR and/or AQP4 (Fig. 4B). This was accompanied by an increase in phospho-AQP4 in the germinal niche (Fig. 4C). Conversely, i.v. injection of muscimol led to an overall decrease in phospho-AQP4 (Fig. 4C), which was paralleled by an increase in the coexpression of EGFR and AQP4 at the cell surface (Fig. 4B). The analysis by immunoprecipitation and immunoblot of the membrane and cytoplasm fractions with AQP4 antibodies confirmed the opposite effects of bicuculline and muscimol i.v. injection on the cellular localization of AQP4 (Fig. 4D). In addition, when whole cell extracts were immunoprecipitated with AQP4 antibodies, separated by electrophoresis, and immunoblotted with phosphoserine antibodies, blockade of GABA<sub>A</sub>Rs led to an increase in serine phosphorylation (Fig. 4E). Importantly, by probing parallel Western blots with either phosphoserine or by AQP4 antibodies, we detected bands of equivalent molecular weight. These experiments strongly indicate that the change in phosphoserine intensity associated with GABA<sub>A</sub>R function concerns serine residues present on the AQP4 molecule and not a coimmunoprecipitated protein, although the latter possibility cannot be formally ruled out. Thus, GABA<sub>A</sub>R signaling modulates AQP4 phosphorylation and its expression at the cell surface *in vivo* and *in vitro*.

**GABA<sub>A</sub>R Function Modulates Osmotic Tension Thereby Affecting Water Exchange in the SEZ**—We next investigated the relationship between GABA<sub>A</sub>R function and cell volume. We first examined the effect of GABA<sub>A</sub>Rs on the response to an osmotic challenge in cells isolated from the neonatal SEZ. Consistent with our previous observations (17), compared with untreated controls, blockade of GABA<sub>A</sub>Rs during dissection decreased the osmotic swelling (Fig. 5A) and the number (Fig. 5B) of E<sup>high</sup> cells, whereas exposure to hypo-osmotic conditions for 5 min caused an opposite outcome. Treatment with bicuculline also significantly delayed the increase in E<sup>high</sup> cells in response to hypo-osmotic treatment, which was significant only 10 min after hypo-osmotic treatment (Fig. 5B). In contrast, a similar treatment with bicuculline and/or hypo-osmotic solution exerted no significant effects in AQP4 KO mice on either osmotic swelling (Fig. 5C) or E<sup>high</sup> cell number (Fig. 5D), confirming that AQP4 represents the main water channel in this population and that the effect of GABA<sub>A</sub>Rs on osmotic swelling depends on AQP4. Importantly, similar results were also observed in E<sup>high</sup> cells loaded with calcein-AM (1 μM) and analyzed by live imaging 1 day after sorting. This analysis revealed that, in comparison with the control group, E<sup>high</sup> cells exposed to bicuculline underwent shrinkage and showed a much slower kinetic of swelling upon hypo-osmotic treatment (Fig. 5, E and

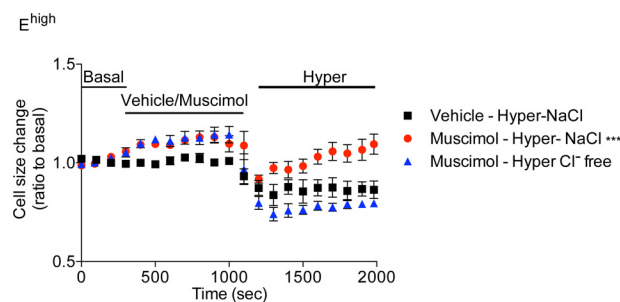


**FIGURE 6. Activation of GABA<sub>A</sub>Rs promotes swelling of EGFR<sup>high</sup> cells and cell volume recovery upon osmotic challenge.** Effect of GABA<sub>A</sub>Rs on the response to osmotic challenge of neonatal E<sup>high</sup> cells that after sorting were cultured in NBA medium for 6–12 h before loading with calcein-AM (1 μM) and live imaging. After 3 min of imaging in basal conditions, muscimol (25 μM) was added to the cells, and recording was performed for another 15 min. Thereafter, the hyper-osmotic solution (400 mosM/kg) with or without Cl<sup>-</sup> was added, and cells were recorded for further 15 min. *n* = 3. Values of the mean curve obtained in basal and treatment conditions were averaged every 100 s and analyzed by two-tailed Student's *t* test.

F). A similar analysis on E<sup>low</sup> cells showed that their size rapidly increased after hypo-osmotic challenge, but it was not affected by exposure to bicuculline (Fig. 5, G and H). Conversely, treatment with muscimol led to a significant increase in cell size in E<sup>high</sup> cells (Fig. 6). Both control and muscimol-treated cells underwent fast shrinkage upon exposure to hyper-osmotic conditions. However, the presence of muscimol led to a significantly faster volume recovery despite the persistence of the increased osmolarity. This effect was likely due to the higher Cl<sup>-</sup> concentration used to obtain hyper-osmotic conditions, as it was not observed upon treatment with a hyper-osmotic solution with a reduced content of Cl<sup>-</sup>. Taken together, these observations show that the direction of the water reflects the movements of Cl<sup>-</sup> across the GABA<sub>A</sub>Rs.

In a similar fashion, sorted P<sup>+</sup> cells displayed a decrease in osmotic tension (Fig. 7A) and a significant reduction in volume (18 ± 1.2% of untreated control; Fig. 7B) when exposed to bicuculline for 30 min in iso-osmolar conditions. Also in isolated P<sup>+</sup> cells blockade of GABA<sub>A</sub>Rs counteracted swelling induced by exposure to hypo-osmotic conditions (Fig. 7A). Moreover, these changes in osmotic swelling upon the various treatments were associated with variations in EGFR expression as already observed in dissociated SEZ cells (Fig. 7C). In contrast, the expression of AQP4 at the cell surface of P<sup>+</sup> cells was decreased by bicuculline, but it was not affected by the change in osmolarity (Fig. 7D). Taken together, these data show that *in vitro* GABA<sub>A</sub>Rs regulate cell volume in iso-osmolar conditions and upon exposure to an osmotic challenge.

Next, we investigated whether GABA<sub>A</sub>R activation affects the response to an osmotic challenge also *in vivo*. Adult mice were i.v. microinjected with vehicle or bicuculline and after 30 min additionally microinjected with iso- or hypo-osmotic solution. After a further 30 min, mice were sacrificed, and changes in the expression of EGFR and AQP4 were analyzed by immunohistofluorescence. Compared with vehicle-microinjected control, the exposure to hypo-osmotic conditions led to a significant increase in the expression of EGFR and a trend increase in AQP4 expression, which was not significant (Fig. 7, E and F). However, mice pre-exposed to bicuculline before i.v. microinjection of hypo-osmotic solution displayed, like mice microin-

## GABA Regulates AQP4 in the SEZ

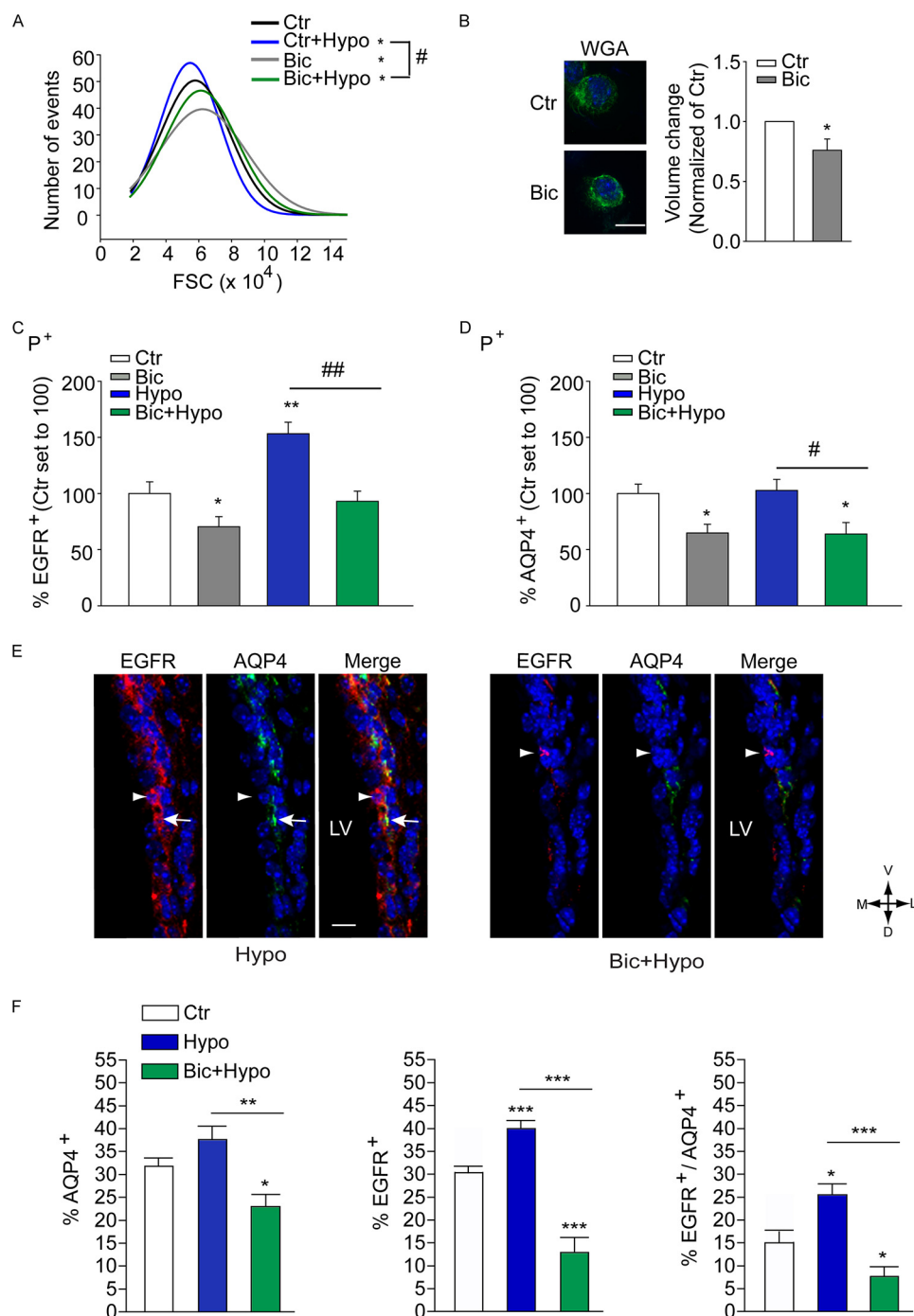


**FIGURE 7. GABA<sub>A</sub>R function modulates osmotic tension and water uptake in response to osmotic challenge.** *A*, representative FACS histograms illustrating the frequency distribution of FSC values of P<sup>+</sup> cells isolated from the P7 SEZ. Curves were fitted by single Gaussian functions whose mean, S.D., and adjusted *R*-squared values were calculated. *B*, spinning disk confocal photomicrographs and quantitative analysis of the volume of P<sup>+</sup> cells treated as indicated before loading with wheat germ agglutinin (WGA)-Alexa 488 and imaging. *Scale bar*, 10  $\mu$ m. *C* and *D*, quantitative analysis of the number of P<sup>+</sup> cells expressing EGFR (*C*) and AQP4 (*D*) at the cell surface after treatment as indicated and immunostaining. After sorting from the P7 SEZ and culturing for 6 h, cells were exposed to bicuculline (*Bic*, 50  $\mu$ M) for 30 min or left untreated. *C* and *D*, before fixation and analysis, cells were exposed for 5 min to normal (*Ctrl*) or hypo-osmotic (*Hypo*) solution. *n*  $\geq$  3. *E*, confocal photomicrographs of coronal sections illustrating a representative example of double immunostaining as indicated and DAPI (*blue*) counterstaining of nuclei. Adult mice were microinjected (*i.v.*) with hypo-osmotic (*Hypo*) solution in the presence or absence of bicuculline as indicated. Immunolabeling was performed without permeabilization. *D*, dorsal; *M*, medial; *L*, lateral; *V*, ventral. *Scale bar*, 15  $\mu$ m. *F*, quantitative analysis of the immunostaining shown in *E*. \* indicates significantly different from control or hypo-osmotic counterparts; *n*  $\geq$  6 mice/group.

jected with bicuculline, a similarly significant reduction in the amount of both membrane EGFR and AQP4 (Fig. 7, *E* and *F*; see also Fig. 4, *A* and *B* for comparison).

To investigate whether blockade of GABA<sub>A</sub>R reduces water uptake under hypo-osmotic stress, which is used as a model of

edema (37, 38), we incubated the whole dissected SEZ with vehicle or bicuculline for 30 min and thereafter exposed the tissue to iso- or hypo-osmotic solution for a further 30 min. As shown in Fig. 8*A*, compared with control tissue exposed to iso-osmotic conditions, tissue incubated in hypo-osmotic medium

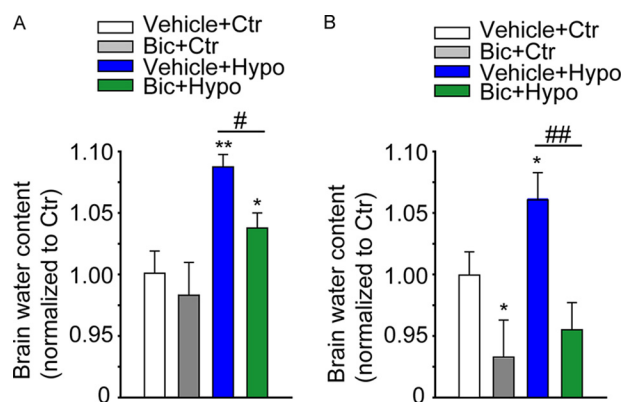


**FIGURE 8. Blockade of GABA<sub>A</sub>R prevents water accumulation in the SEZ upon hypo-osmotic challenge.** Quantitative analyses of the water uptake in the SEZ exposed to the indicated treatments *ex vivo* (A) or *in vivo* (B). A, after dissection, the tissue was incubated with or without bicuculline (Bic, 50  $\mu$ M) for 30 min. Thereafter, tissue was treated with iso- (Ctr) or hypo-osmotic (Hypo) solution for a further 30 min, all at 37 °C. B, 30 min after i.v. microinjection with vehicle or bicuculline (30 pmol), iso- (Ctr) or hypo-osmotic solution was additionally microinjected as indicated. After a further 30 min, mice were sacrificed, and the SEZ was dissected and processed for the analysis of the water content. \* indicates significantly different from vehicle + control group (ANOVA);  $n \geq 3$ .

displayed an increase (~6%) in water content. Moreover, pretreatment with bicuculline reduced water uptake in the tissue group exposed to hypo-osmotic but not iso-osmotic conditions. Similar results were observed *in vivo* upon microinjection of bicuculline and hypo-osmotic solution into the lateral ventricle (Fig. 8B), showing that also in this case blockade of GABA<sub>A</sub>R can prevent the increase in water uptake in SEZ induced by injection of hypo-osmotic solution. Thus, blockade of GABA<sub>A</sub>R can serve as a mean to rescue water disequilibrium in the SEZ.

## DISCUSSION

We have previously shown that GABA<sub>A</sub>R activation leads to hyperpolarization and osmotic swelling in SEZ stem cells causing expression of EGFR at the cell surface (17). In this study, we provide evidence that in addition to Cl<sup>-</sup> influx activation of GABA<sub>A</sub>R in SEZ precursors also modulates the surface expression of AQP4. We found that the effect of GABA<sub>A</sub>R activation on osmotic tension not only affected EGFR expression in the SEZ but also water retention. As the primary function of AQP4 concerns the regulation of water exchange through the various compartments of the brain (39), it is very likely that the effect of bicuculline on water retention is a consequence of its modulation of AQP4 expression.

Within the SEZ, the AQP4 channel is expressed in the ependymal layer, where it contributes to maintain its integrity, and in the underlying germinal epithelium in precursors and to a lesser extent in niche astrocytes (20). Consistent with this, we found that in neonatal mice the expression of AQP4 is mainly confined to the populations of P<sup>+</sup>/E<sup>low</sup> and P<sup>+</sup>/E<sup>high</sup> cells, which at this age include most of the ependymal cells as well as NSCs (9). The latter are particularly enriched within the P<sup>+</sup>/E<sup>high</sup> population representing activated NSCs (7–9). In contrast, prospectively isolated neonatal P<sup>-</sup>/E<sup>high</sup> TAPs and P<sup>-</sup>/E<sup>low</sup> neuroblasts expressed very low levels of AQP4 mRNA, showing that the AQP4 is rapidly down-regulated during neu-

ronal differentiation. However, at the protein level the differences between P<sup>+</sup> and P<sup>-</sup> cells were reduced, suggesting a relative stability of the water channel. Moreover, in culture conditions the AQP4 immunoreactivity was observed in most of the cells, which likely reflects the selection for precursor cells in culture conditions.

In the SEZ, functional GABA<sub>A</sub>R currents have been recorded from both precursors and more mature neuronal progenitors, although their size and directions differ in the two cell groups (17). In immature neural precursors, GABA<sub>A</sub>R currents are hyperpolarizing and relatively small, which may lead to a requirement for proximity within the cell between the anionic channel and the targeted proteins. Indeed, our data indicate that GABA<sub>A</sub>R and AQP4 localize closely. Previous analyses have shown that the localization of AQP4 at the end-feet of perivascular astrocytes is dependent on its interaction with syntrophin within the dystrophin-glycoprotein complex (40, 41). Because the dystrophin complex also plays a role in the assembly of the GABA<sub>A</sub>Rs, it is possible that both channels interact with the dystrophin complex. However, this possibility may only concern the subset of SEZ astrocytes, including P<sup>+</sup> NSCs. In fact, although globules containing dystroglycan and other dystrophin-glycoprotein complex components have been observed in ependymal cells, the interaction between dystrophin-glycoprotein complex and AQP4 appears not essential for the localization of AQP4 within this cell group (42).

Multiple kinases and phosphorylation sites have been involved in the regulation of the phosphorylation status of AQP4 (28, 29). For example, at the invasive hedges of gliomas, PKC is closely localized to clusters of AQP4 and Cl<sup>-</sup> channels and transporters. In this system, PKC activation inhibits tumor cell migration and invasiveness by promoting AQP4 phosphorylation on serine 180 (43). Instead, in kidney epithelial cells phosphorylation of serine 279 by casein kinase II leads to lysosomal targeting and degradation of the water channel (32). In contrast, we found here that GABA<sub>A</sub>R activation decreased phospho-AQP4 and enhanced the expression of the water channel at the cell surface, which was prevented by BFA. This suggests that the GABAergic regulation of phospho-AQP4 modulates the anterograde transport of AQP4. Thus, the mechanisms underlying the regulation of the water channel are complex and may be dependent on the cellular context.

In contrast to AQP4, our data indicate that GABA<sub>A</sub>Rs regulate surface EGFR expression mainly by affecting osmotic tension, as endogenous GABA<sub>A</sub>R signaling maintains EGFR expression only within P<sup>+</sup> cells that express high levels of the water channel. Moreover, blockade of GABA<sub>A</sub>Rs did not affect EGFR expression in precursors isolated from AQP4 KO mice, and EGFR expression was similarly enhanced by forced activation of GABA<sub>A</sub>Rs and hypo-osmotic treatment. However, the exposure to hypo-osmotic conditions affected EGFR expression also in AQP4<sup>-</sup> cells. It is unlikely that these AQP4<sup>-</sup> cells represent either neuroblasts or SEZ astrocytes, as they do not express EGFR. Rather they may represent cells in the process of down-regulating EGFR before differentiating into neuroblasts. This is consistent with our previous findings showing that the amount of EGFR transcripts and protein peaks within the population of E<sup>high</sup> cells and that EGFR expression is rapidly down-

regulated during the transition from pre-neuroblasts to neuroblasts (6). Thus, our findings unveil a new mechanism by which GABA<sub>A</sub>Rs regulate osmotic tension in the SEZ precursors, thereby modulating EGFR expression and water exchange in this region.

*Acknowledgments*—The AQP4 KO mice were generously provided by Dr. Erlend A. Nagelhus, Institute of Basic Medical Sciences, University of Oslo, Norway.

### REFERENCES

- Lois, C., García-Verdugo, J. M., and Alvarez-Buylla, A. (1996) Chain migration of neuronal precursors. *Science* **271**, 978–981
- Mirzadeh, Z., Merkle, F. T., Soriano-Navarro, M., Garcia-Verdugo, J. M., and Alvarez-Buylla, A. (2008) Neural stem cells confer unique pinwheel architecture to the ventricular surface in neurogenic regions of the adult brain. *Cell Stem Cell* **3**, 265–278
- Dubreuil, V., Marzesco, A. M., Corbeil, D., Huttner, W. B., and Wilsch-Bräuninger, M. (2007) Midbody and primary cilium of neural progenitors release extracellular membrane particles enriched in the stem cell marker prominin-1. *J. Cell Biol.* **176**, 483–495
- Coskun, V., Wu, H., Bianchi, B., Tsao, S., Kim, K., Zhao, J., Biancotti, J. C., Hutnick, L., Krueger, R. C., Jr., Fan, G., de Vellis, J., and Sun, Y. E. (2008) CD133<sup>+</sup> neural stem cells in the ependyma of mammalian postnatal forebrain. *Proc. Natl. Acad. Sci. U.S.A.* **105**, 1026–1031
- Doetsch, F., Petreanu, L., Caille, I., Garcia-Verdugo, J. M., and Alvarez-Buylla, A. (2002) EGF converts transit-amplifying neurogenic precursors in the adult brain into multipotent stem cells. *Neuron* **36**, 1021–1034
- Cesetti, T., Obernier, K., Bengtson, C. P., Fila, T., Mandl, C., Hözl-Wenig, G., Wörner, K., Eckstein, V., and Ciccolini, F. (2009) Analysis of stem cell lineage progression in the neonatal subventricular zone identifies EGFR<sup>+</sup>/NG2<sup>-</sup> cells as transit-amplifying precursors. *Stem Cells* **27**, 1443–1454
- Carrillo-García, C., Suh, Y., Obernier, K., Hözl-Wenig, G., Mandl, C., and Ciccolini, F. (2010) Multipotent precursors in the anterior and hippocampal subventricular zone display similar transcription factor signatures but their proliferation and maintenance are differentially regulated. *Mol. Cell. Neurosci.* **44**, 318–329
- Obernier, K., Simeonova, I., Fila, T., Mandl, C., Hözl-Wenig, G., Monaghan-Nichols, P., and Ciccolini, F. (2011) Expression of Tlx in both stem cells and transit amplifying progenitors regulates stem cell activation and differentiation in the neonatal lateral subependymal zone. *Stem Cells* **29**, 1415–1426
- Khatri, P., Obernier, K., Simeonova, I. K., Hellwig, A., Hözl-Wenig, G., Mandl, C., Scholl, C., Wöfl, S., Winkler, J., Gaspar, J. A., Sachinidis, A., and Ciccolini, F. (2014) Proliferation and cilia dynamics in neural stem cells prospectively isolated from the SEZ. *Sci. Rep.* **4**, 3803
- Cesetti, T., Ciccolini, F., and Li, Y. (2011) GABA not only a neurotransmitter: osmotic regulation by GABA(A)R signaling. *Front. Cell. Neurosci.* **6**, 3
- Suh, H., Deng, W., and Gage, F. H. (2009) Signaling in adult neurogenesis. *Annu. Rev. Cell Dev. Biol.* **25**, 253–275
- Vicini, S. (2008) The role of GABA and glutamate on adult neurogenesis. *J. Physiol.* **586**, 3737–3738
- Nguyen, L., Malgrange, B., Breuskin, I., Bettendorff, L., Moonen, G., Belachew, S., and Rigo, J. M. (2003) Autocrine/paracrine activation of the GABA(A) receptor inhibits the proliferation of neurogenic polysialylated neural cell adhesion molecule-positive (PSA-NCAM<sup>+</sup>) precursor cells from postnatal striatum. *J. Neurosci.* **23**, 3278–3294
- Bolteus, A. J., and Bordey, A. (2004) GABA release and uptake regulate neuronal precursor migration in the postnatal subventricular zone. *J. Neurosci.* **24**, 7623–7631
- Apra, J., and Calegari, F. (2012) Bioelectric state and cell cycle control of mammalian neural stem cells. *Stem Cells Int.* **2012**, 816049
- Andäng, M., Hjerling-Leffler, J., Moliner, A., Lundgren, T. K., Castelo-Branco, G., Nanou, E., Pozas, E., Bryja, V., Halliez, S., Nishimaru, H., Wilbertz, J., Arenas, E., Koltzenburg, M., Charnay, P., El Manira, A., Ibañez, C. F., and Ernfrors, P. (2008) Histone H2AX-dependent GABA(A) receptor regulation of stem cell proliferation. *Nature* **451**, 460–464
- Cesetti, T., Fila, T., Obernier, K., Bengtson, C. P., Li, Y., Mandl, C., Hözl-Wenig, G., and Ciccolini, F. (2011) GABA receptor signaling induces osmotic swelling and cell cycle activation of neonatal prominin<sup>+</sup> precursors. *Stem Cells* **29**, 307–319
- Ming, G. L., and Song, H. (2011) Adult neurogenesis in the mammalian brain: significant answers and significant questions. *Neuron* **70**, 687–702
- Venero, J. L., Vizuete, M. L., Machado, A., and Cano, J. (2001) Aquaporins in the central nervous system. *Prog. Neurobiol.* **63**, 321–336
- Cavazzin, C., Ferrari, D., Facchetti, F., Russignan, A., Vescovi, A. L., La Porta, C. A., and Gritti, A. (2006) Unique expression and localization of aquaporin-4 and aquaporin-9 in murine and human neural stem cells and in their glial progeny. *Glia* **53**, 167–181
- Kong, H., Fan, Y., Xie, J., Ding, J., Sha, L., Shi, X., Sun, X., and Hu, G. (2008) AQP4 knockout impairs proliferation, migration and neuronal differentiation of adult neural stem cells. *J. Cell Sci.* **121**, 4029–4036
- Haj-Yasein, N. N., Vindedal, G. F., Eilert-Olsen, M., Gundersen, G. A., Skare, Ø., Laake, P., Klungland, A., Thorén, A. E., Burkhardt, J. M., Ottersen, O. P., and Nagelhus, E. A. (2011) Glial-conditional deletion of aquaporin-4 (Aqp4) reduces blood-brain water uptake and confers barrier function on perivascular astrocyte endfeet. *Proc. Natl. Acad. Sci. U.S.A.* **108**, 17815–17820
- Papadopoulos, M. C., and Verkman, A. S. (2007) Aquaporin-4 and brain edema. *Pediatr. Nephrol.* **22**, 778–784
- Thrane, A. S., Rappold, P. M., Fujita, T., Torres, A., Bekar, L. K., Takano, T., Peng, W., Wang, F., Rangroo Thrane, V., Enger, R., Haj-Yasein, N. N., Skare, Ø., Holen, T., Klungland, A., Ottersen, O. P., Nedergaard, M., and Nagelhus, E. A. (2011) Critical role of aquaporin-4 (AQP4) in astrocytic Ca<sup>2+</sup> signaling events elicited by cerebral edema. *Proc. Natl. Acad. Sci. U.S.A.* **108**, 846–851
- Vizuete, M. L., Venero, J. L., Vargas, C., Ilundáin, A. A., Echevarría, M., Machado, A., and Cano, J. (1999) Differential upregulation of aquaporin-4 mRNA expression in reactive astrocytes after brain injury: potential role in brain edema. *Neurobiol. Dis.* **6**, 245–258
- Taniguchi, M., Yamashita, T., Kumura, E., Tamatani, M., Kobayashi, A., Yokawa, T., Maruno, M., Kato, A., Ohnishi, T., Kohmura, E., Tohyama, M., and Yoshimine, T. (2000) Induction of aquaporin-4 water channel mRNA after focal cerebral ischemia in rat. *Brain Res. Mol. Brain Res.* **78**, 131–137
- Saadoun, S., Papadopoulos, M. C., Davies, D. C., Krishna, S., and Bell, B. A. (2002) Aquaporin-4 expression is increased in oedematous human brain tumours. *J. Neurol. Neurosurg. Psychiatry* **72**, 262–265
- Zelenina, M., Zelenin, S., Bondar, A. A., Brismar, H., and Aperia, A. (2002) Water permeability of aquaporin-4 is decreased by protein kinase C and dopamine. *Am. J. Physiol. Renal Physiol.* **283**, F309–F318
- Carmosino, M., Procino, G., Tamma, G., Mannucci, R., Svelto, M., and Valentini, G. (2007) Trafficking and phosphorylation dynamics of AQP4 in histamine-treated human gastric cells. *Biol. Cell* **99**, 25–36
- Ciccolini, F., and Svendsen, C. N. (1998) Fibroblast growth factor 2 (FGF-2) promotes acquisition of epidermal growth factor (EGF) responsiveness in mouse striatal precursor cells: identification of neural precursors responding to both EGF and FGF-2. *J. Neurosci.* **18**, 7869–7880
- Söderberg, O., Gullberg, M., Jarvius, M., Ridderstråle, K., Leuchowius, K. J., Jarvius, J., Wester, K., Hydbring, P., Bahram, F., Larsson, L. G., and Landegren, U. (2006) Direct observation of individual endogenous protein complexes in situ by proximity ligation. *Nat. Methods* **3**, 995–1000
- Johnstone, S. R., Kroncke, B. M., Straub, A. C., Best, A. K., Dunn, C. A., Mitchell, L. A., Peskova, Y., Nakamoto, R. K., Koval, M., Lo, C. W., Lampe, P. D., Columbus, L., and Isakson, B. E. (2012) MAPK phosphorylation of connexin 43 promotes binding of cyclin E and smooth muscle cell proliferation. *Circ. Res.* **111**, 201–211
- Madrid, R., Le Maout, S., Barrault, M. B., Janvier, K., Benichou, S., and Mérot, J. (2001) Polarized trafficking and surface expression of the AQP4 water channel are coordinated by serial and regulated interactions with different clathrin-adaptor complexes. *EMBO J.* **20**, 7008–7021
- Kadohira, I., Abe, Y., Nuriya, M., Sano, K., Tsuji, S., Arimitsu, T., Yo-

- shimura, Y., and Yasui, M. (2008) Phosphorylation in the C-terminal domain of Aquaporin-4 is required for Golgi transition in primary cultured astrocytes. *Biochem. Biophys. Res. Commun.* **377**, 463–468
35. Gunnarson, E., Zelenina, M., and Aperia, A. (2004) Regulation of brain aquaporins. *Neuroscience* **129**, 947–955
36. Nebenführ, A., Ritzenthaler, C., and Robinson, D. G. (2002) Brefeldin A: deciphering an enigmatic inhibitor of secretion. *Plant Physiol.* **130**, 1102–1108
37. Risher, W. C., Andrew, R. D., and Kirov, S. A. (2009) Real-time passive volume responses of astrocytes to acute osmotic and ischemic stress in cortical slices and *in vivo* revealed by two-photon microscopy. *Glia* **57**, 207–221
38. Nase, G., Helm, P. J., Enger, R., and Ottersen, O. P. (2008) Water entry into astrocytes during brain edema formation. *Glia* **56**, 895–902
39. Benfenati, V., and Ferroni, S. (2010) Water transport between CNS compartments: functional and molecular interactions between aquaporins and ion channels. *Neuroscience* **168**, 926–940
40. Bragg, A. D., Amiry-Moghaddam, M., Ottersen, O. P., Adams, M. E., and Froehner, S. C. (2006) Assembly of a perivascular astrocyte protein scaffold at the mammalian blood-brain barrier is dependent on  $\alpha$ -syntrophin. *Glia* **53**, 879–890
41. Binder, D. K., Nagelhus, E. A., and Ottersen, O. P. (2012) Aquaporin-4 and epilepsy. *Glia* **60**, 1203–1214
42. Nicchia, G. P., Rossi, A., Nudel, U., Svelto, M., and Frigeri, A. (2008) Dystrophin-dependent and -independent AQP4 pools are expressed in the mouse brain. *Glia* **56**, 869–876
43. McCoy, E. S., Haas, B. R., and Sontheimer, H. (2010) Water permeability through aquaporin-4 is regulated by protein kinase C and becomes rate-limiting for glioma invasion. *Neuroscience* **168**, 971–981